REVIEWS OF TRUE AMPLITUDE COMPUTATIONS IN PLANE-LAYERED STRUCTURES

LARRY W. MARKS † and F. HRON †

ABSTRACT

Numerical modelling in seismology is playing an increasing role in exploration geophysics. Ray theories which decompose the wave field into contributions attributed to individual rays, represent a very efficient method for computation of synthetic seismograms. An important initial step in utilizing any ray method is the generation and selection of individual rays constituting a partial ray expansion. If models consist of plane, parallel layers with no lateral inhomogeneities, the implementation of the concepts of kinematic analogs (rays which have identical travel-time properties) and dynamic analogs (rays which have identical travel-time and amplitude-distance properties) is essential. It will be shown that individual "events" in the seismogram correspond to the arrivals of individual groups of kinematic analogs, whose dynamic properties differ significantly from those of individual rays.

Asymptotic ray theory yields easily computable correct results for receiver distances far from the critical point. At the critical point, unfortunately, this theory breaks down and predicts an infinite amplitude for the head wave. However, both field studies and theoretical investigations based on wave methods indicate that it is in this region that rays convey the maximum amount of energy to the receiver. To investigate amplitudes in this important zone, a new approach to amplitude computation is presented. In this technique, the interference wave, resulting from the composite of the reflected wave and head wave, is expressed in terms of a Weber function. The effect of multiply reflected head waves may also be included in this method. Numerical results show that amplitudes of dynamic groups calculated via this method oscillate about asymptotic ray theoretical values and converge outside the interference zone. Consequently, a combination of both techniques represents a very efficient tool for the computation of synthetic seismograms or amplitude-distance characteristics.

INTRODUCTION

Ray methods of decomposing the seismic wave field into individual ray contributions provide excellent tools for modelling seismic disturbances. These techniques synthesize wave propagation in three stages: first, the selection of a physically realistic set of rays to participate in the construction of a theoretical seismic trace; second, the computation of the arrival time of these rays at a receiver at any prescribed epicentral distance; and finally, the amplitude of the ground motion at the receiver.

A very efficient method of ray amplitude computation is based upon asymptotic ray theory, an outline of which is contained in Appendix A. The interested reader should consult Hron and Kanasewich (1971) or Cerveny and Ravindra (1971). This ray theory expresses the solution to the wave equation

†Institute of Earth and Planetary Physics, Department of Physics University of Alberta Edmonton, Alberta, Canada T6G 2J1

and boundary conditions in the form of an asymptotic series in inverse powers of frequency. This formulation renders the theory applicable to high frequency waves. The ray theory can easily be applied to the generation of synthetic seismograms in plane, parallel layered, homogeneous media. One deficiency of this approach is the infinite amplitude that asymptotic ray theory predicts for head waves at the critical point. This phenomenon renders these theoretical head waves inoperative within the interference zone, which is the region immediately beyond the critical point. It is within this region that the maximum energy is transmitted to the surface. The end of the interference zone is defined as that epicentral distance at which the difference in time between the arrivals of reflected and head waves is equal to the time duration of the source pulse. Clearly, the length of the interference zone is inversely proportional to source frequency. Methods for computing interference zone lengths are described in Cerveny (1962b). Asymptotic ray theory was employed to produce Figure 1, which is an amplitude-distance curve for a reflected harmonic P wave (PP) and its associated P type (PPP) and S type (PSP) head waves. These curves were determined through the direct evaluation of equation A-3 and A-4. The singularities of the head wave amplitudes at the critical points is clear. The two critical points (marked R_{cp} and R_{cs}) and the ends of the interference zones (marked R_{ip} and R_{is}) are shown. The frequency, F, of the harmonic source pulse is 15 Hz. The model for which the amplitude computations shown in Figures 1-5 were performed is Model 1 listed in Table 1. In the ray sketches given in the upper right hand corners of these amplitude results, a solid (dashed) line denotes propagation as a P(S) wave.

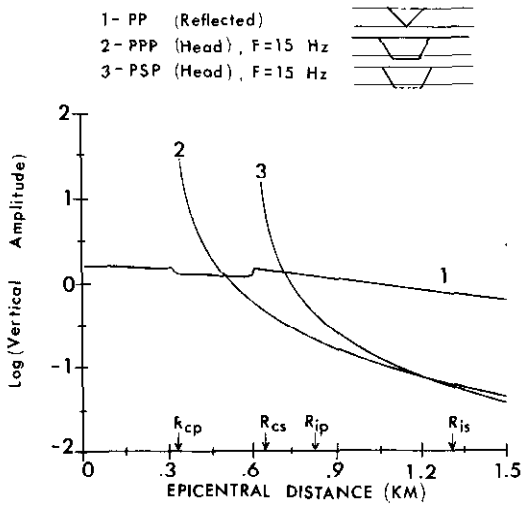

Fig. 1. Common logarithm of vertical amplitude versus epicentral distance for waves in the top liquid layer in Model 1. All amplitudes are computed by asymptotic ray theory. The critical distances for P and S head waves are marked by R_{cp} and R_{cs}, respectively. The ends of the interference zones are marked by R_{ip} and R_{is}.

TABLE 1
Model 1

Layer Number	P wave Velocity km/sec	S wave Velocity km/sec	Volume density g/cm^3	Thickness km
1	1.500	0	1.0	0.5
2	5.000	2.887	2.6	4.5
3	6.00	3.464	2.8	15.0
4	7.200	4.157	3.1	10.0
Half-space	8.200	4.734	3.4	∞

According to Kosminskaya, 1970, personal communication.

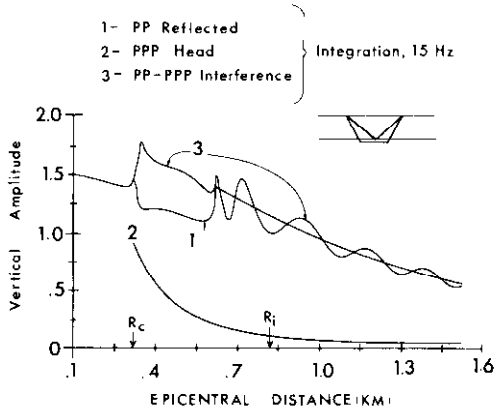

Fig. 2. Vertical amplitude-distance curves computed by numerical integration for a reflected P wave (PP), its associated P head wave (PPP) and the composite interference wave (PP-PPP). The computations were performed for the top liquid layer of Model 1.

Within the interference zone the reflected wave and the head wave both exist and cannot be distinguished from each other. A method, albeit costly, of determining the amplitudes of these waves within the interference zone is a direct numerical integration of the potential solutions to the wave equation. Following the theory developed in Brekhovskikh (1960) one may obtain an integral form for the vertical displacement of a wave at the free surface. This is

$$A(r) = \frac{ik}{2} e^{-i\omega t} \int_{-\infty}^{\infty} \sigma H_0^{(1)}(krq) e^{ikB(q)} q\,dq \qquad (1)$$

where $k = \omega/a_1$ is the wave number in the first layer, $H_0^{(1)}$ is the Hankel function of the first kind and zeroth order and B(q) is the phase function of the ray. The term σ represents the product of all complex coefficients corresponding to the ray's interaction with interfaces in the medium. The integration path may be deformed (Cerveny, 1965) so that a saddle point approximation utilizing the asymptotic expansion for the Hankel function is applicable. Contributions corresponding to the reflected wave stem from integration along a path parametrized in the real variable p as

$$(1-q^2)^{\frac{1}{2}} = (1-x^2)^{\frac{1}{2}} + pe^{-i\pi/4}, \quad -\infty<p<\infty, \quad x = \sin\theta_1 \qquad (2)$$

and x is the (real valued) parameter of the ray arriving at the epicentral distance r. Head wave contributions are obtained by integrating along a branch cut parametrized as

$$(1-q^2)^{\frac{1}{2}} = (1-x^{*2})^{\frac{1}{2}} + pe^{-i\pi/4}, \quad 0\le p<\infty \qquad (3)$$

where x^* is the parameter corresponding to critical reflection at the bottoming interface.

The actual integrations along these paths were performed by cautious Romberg extrapolation using an algorithm proposed by de Boor (1971). Curves 1 and 2 are the amplitudes of the reflected P wave (PP) and the P head wave (PPP) determined by this method. Curve 3 in this diagram is the composite interference wave amplitude. The source frequency is 15 Hz. The advantage of this integral approach is that the head wave has a finite amplitude at the critical point. However, the cost of computation is roughly two orders of magnitude greater than that for asymptotic ray theory. A rather interesting feature of the interference wave is the oscillatory nature of the amplitude. These oscillations will also be found in the amplitude expressed in terms of the Weber function as a result of saddle point approximations of contour integrals in the wave solution.

INTERFERENCE AMPLITUDES COMPUTED WITH THE HELP OF THE WEBER FUNCTION

A computationally suitable approach to constructing amplitude-distance curves for reflected-head wave interference has recently been derived (Marks 1976, Marks and Hron 1979) based on the original method of Cerveny (1962a, 1965, 1967). This technique allows one to express the amplitude-distance curves of interference waves in terms of a Weber function (or rather, a Parabolic Cylinder function). The mathematical properties of this function can be found in Magnus and Oberhettinger (1949) and Kireyeva and Karpov (1961). The formula for these amplitudes as a function of epicentral distance r is (Appendix B)

$$A = \frac{\sigma}{Q}\left\{R^M(x_L) - \left(\frac{x_1^{*3}(1-x_1^{*2})}{k(r-\tilde{r}^*)}\right)^{\frac{1}{2}} M\Gamma \frac{v_{L+1}}{a_1} cR^{M-1}(x_L^*)G(y)\right\} \qquad (4)$$

where the following notation has been used:

Q geomecrical spreading of the reflected wave,

R reflection coefficient corresponding to the bottoning reflection of the ray,

σ product of all other reflection and transmission coefficients,

$$x_1^* = a_1/v_{L+1}, \quad x_L^* = a_L/v_{L+1}$$

a_i, b_i compressional or shear wave velocity in the i-th layer.

v_{L+1} velocity of propagation of refracted segment of head wave,

$k = \omega/a_1$ wave number in top layer,

L deepest layer that the ray penetrates,

$$c = \begin{cases} \dfrac{b_{L+1}}{a_{L+1}} & \text{for S type head waves,} \\ 1 & \text{for P type head waves,} \end{cases}$$

Γ head wave coefficient

M multiplicity factor; equal to the number of reflections from the deepest interface,

$$y = \begin{cases} \left(\dfrac{k(r-\tilde{r})}{2x_1^3}\right)^{1/2}\left((1-x_1^{*2})^{1/2}-(1-x_1^{2})^{1/2}\right) & \text{for } r<r^* \\ (\omega\Delta t)^{1/2} & \text{for } r\geq r^*, \end{cases}$$

x_i ray parameter for the reflected wave in the i-th layer,

r^* critical distance,

Δt difference in arrival time between reflected and head wave,

$\tilde{r}$ $\tilde{r}^*$ with x_1 exchanged for x_1^*, and

$$G(y) = 2^{1/2}\exp\left(i\frac{\pi}{8} - i\frac{y^2}{2}\right) D_{1/2}(y(i-1))-i2^{3/4}y^{1/2}.$$

$$\tilde{r}^* = x_1^{*3}\cdot\sum_{i=1}^{L}\left(\frac{h_i N_{Pi}\left(\frac{a_1^2}{a_i^2}-1\right)}{\left(\frac{a_1^2}{a_i^2}-x_1^{*2}\right)^{3/2}} + \frac{h_i N_{Si}\left(\frac{a_1^2}{b_i^2}-1\right)}{\left(\frac{a_1^2}{b_i^2}-x_1^{*2}\right)^{3/2}}\right)$$

h_i thickness of i-th layer,

N_{Pi}, N_{Si} number of P or S ray segments in the i-th layer .

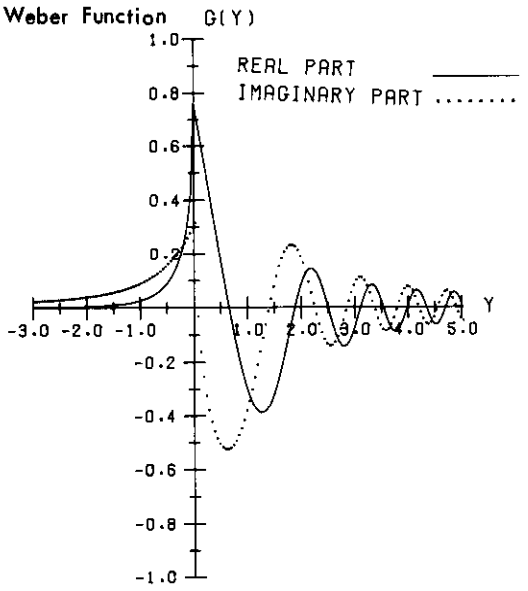

Fig. 3. The graph of the complex valued function G(y) of real variable y.

The complex valued function G(y) versus y is shown in Figure 3. The algorithm for its numerical computation is discussed in Marks and Hron (1977). From the above definition one sees that at the critical point y is equal to 0 and it increases beyond that point. The cost of evaluating equation (4) may be made comparable to that of asymptotic ray theory. This can be accomplished by computing the function G(y) initially for a large finely sampled range of y (say $y\epsilon(-3,5)$) and later retrieving the desired values from a computer disc file in direct input mode during computation.

One can observe the oscillatory nature of the function G(y) in the amplitude-distance curves for interference reflected-head waves. Figure 4 displays the amplitude-distance curves for an unconverted P wave reflected from the third interface of Model 1 (amplitude curve shown dashed). The computation of curve 1 was performed by asymptotic ray theory. The remaining two amplitude curves were computed for the interference reflected-head wave for frequencies of 30 and 45 Hz of the harmonic source of unit amplitude using the Weber function approximation. These amplitudes oscillate about the amplitude of the reflected wave (curve 1). The period of the oscillations decreases with increased fre-

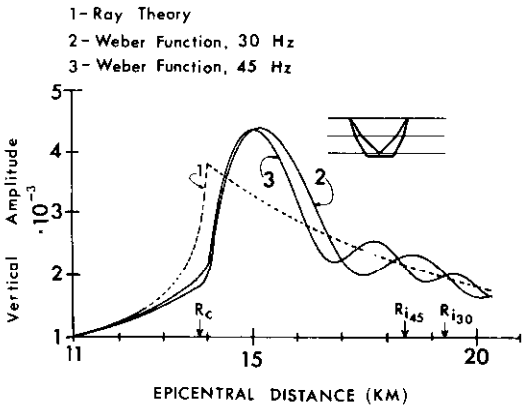

Fig. 4. Interference wave amplitude computed by the Weber function approach for harmonic sources of frequencies 30 and 45 Hz (solid curves) compared with the reflected wave amplitude computed by asymptotic ray theory. The rays are sketched in the upper right hand corner. The computation was carried out for the top two layers of Model 1.

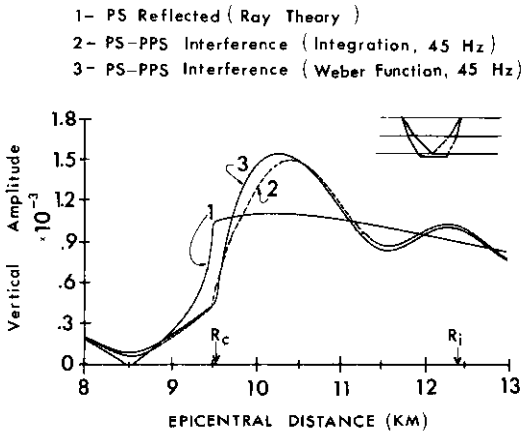

Fig. 5. Comparison of amplitudes computed by three methods (asymptotic ray theory, numerical integration and the Weber function) for Model 1. The rays under consideration are a converted PS reflection and a PPS head wave.

quency. It is interesting to note the locations of maximum amplitudes in these results. Asymptotic ray theory predicts a maximum for the reflected wave amplitude exactly at the critical point. However, the effect of the head wave is to shift this maximum of the interference wave somewhat beyond the critical point. The separation between the point of maximum amplitude and the critical point diminishes with increasing frequency, as does the value of this maximum since the asymptotic ray theory result can be regarded as the high frequency limit. This phenomenon was originally reported by Cerveny (1965).

To determine the validity of the Weber function approach one must compare it with the direct numerical integration. This is shown in Figure 5 for a converted PS reflection. Curve 2 (shown dashed) is the interference wave amplitude produced by numerical integration whereas curve 3 is produced by the Weber function. The matching between the two techniques is very close throughout the displayed region. One observes that amplitudes computed by either method oscillate about the amplitude computed from ray theory (curve 1) of the purely reflected wave (which, incidentally, may be used as the simplest approximation of the interference reflected-head wave (Hron and Kanasewich 1971)).

Dynamic properties of seismic waves in both temporal and spatial domains are best visualized in the form of synthetic seismograms. Figure 6 is a set of synthetic seismograms for Model 1 where we have limited the partial ray expansion to only those rays which have two P ray segments in the uppermost layer. Under this restriction, only three waves can contribute. These are the PP reflected wave, the PPP and PSP head waves, labelled respectively 1, 1.1, and 1.2 on the synthetic section. The dashed lines indicate the travel-time curve of these rays. The amplitudes of the pulses in Figure 6 were computed by asymptotic ray theory outside the interference zone and by the Weber function approach within. The critical points for PPP and PSP head waves are at R = 0.31 and 0.61 km, respectively. The lengths of the corresponding interference zones are 0.53 and 0.65 km. The source pulse, of predominant frequency F = 15 Hz, was taken to be one of several often used in synthetic seismogram computation, (Berzon et al., 1962)

$$S(t) = \sin(2\pi Ft)\exp(-(2\pi Ft/g)^2) \qquad (5)$$

where g = 2.0 and t is time.

In conclusion, this section of the paper has presented results of a method for computing the amplitude of the interference reflected-head wave within the interference zone. The

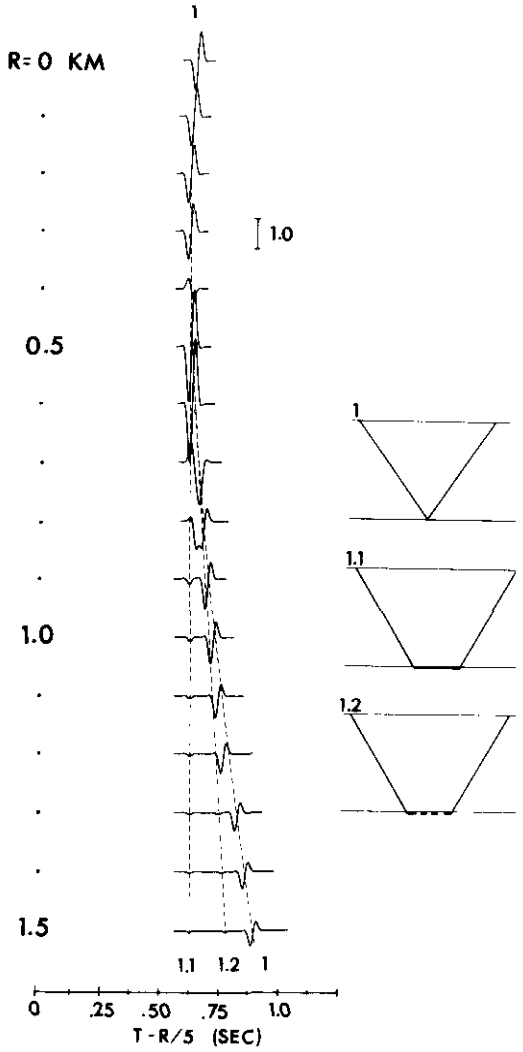

Fig. 6. Separation of the PPP and PSP head wave pulses (1.1 and 1.2) from the reflected P wave pulse (1) in Model 1. The predominant frequency of the pulse is 15 Hz, and the reducing velocity is 5 km/sec. The first and second critical points are located at 0.31 km and 0.61 km, respectively. The dashed lines indicate the travel times of the three waves involved.

advantages of this method are its low computational cost and its non-singular behaviour at the critical point. Numerical ray generation, discussed next, may be used in conjunction with this approach and asymptotic ray theory to create synthetic seismograms for multi-layered models.

Kinematic And Dynamic Analogs

If an earth model is chosen which has no lateral inhomogeneities inside the layers of constant thickness, the concepts of kinematic and dynamic analogs may be implemented. These algorithms provide a large set of rays for the production of synthetic seismograms in the most efficient arrangement.

Those waves which travel from source to receiver along different paths, but with identical travel-times are kinematically equivalent and are termed kinematic analogs. Hron (1972) showed that geometrical spreading and ray parameter are also the same for each kinematically equivalent group, thus making amplitude computation more efficient. This group of analogs may be further subdivided into groups of waves which have identical amplitude-distance properties. The members within each of these subgroups are termed dynamic analogs. The computational efficiency lies in this subdivision. If we know the number of dynamic analogs, say N_D, within a subgroup and the amplitude, say A_D, of only one of them, then the total amplitude of the subgroup is $N_D \cdot A_D$. By adding up the amplitudes of all the dynamic subgroups, the total amplitude of the set of kinematic analogs is determined.

Since there are in fact an infinite number of rays propagating between source and receiver, we must have some criterion for limiting the number of rays which we shall actually examine within a given time window. For this purpose, we have chosen this parameter to be the total number of ray segments, K, within each ray. A FORTRAN program has been written which will generate all rays with up to K segments and automatically partition each kinematic group into the appropriate number of dynamic analogs.

Methods for generating unconverted as well as once converted phases (from P to S mode of propagation or vice versa) have been discussed by Hron (1972). Consider a medium consisting of L homogeneous layers separated by plane parallel interfaces. These interfaces are numbered in the downward direction with the j−th interface separating the layers j−1 and j. Suppose that a ray has been generated with $2n_j$ ($j = 1, \ldots, J$) ray segments in each of the $J \leq L$ layers through which it passes. We may then denote the number of reflections

from the J+1−th interface when the incident ray is in the j−the layer by m_j. Clearly, this number must satisfy

$$\mathrm{Max}(0, n_j - n_{j+1}) \le m_j \le n_j - 1, \quad j = 1, \ldots, J-1. \tag{6}$$

A symbol for a kinematically equivalent group may be written as $(n_1, n_2, \ldots, n_J)$. A symbol for a group of dynamic analogs may be written as $(n_1, n_2, \ldots, n_j; m_1, \ldots, m_{j-1})$ since these numbers will uniquely determine the amplitude-distance curve of the wave. Let us define $\Lambda(m_j)$ as the number of integers which cause m_j to satisfy equation (6). The number of dynamic subgroups within the kinematic group is then.

$$N_{DS}(n_1, \ldots n_J) = \prod_{j=1}^{J-1} \Lambda(m_j). \tag{7}$$

Hron (1972) has shown that the number of individual waves in the dynamic subgroup defined by $(n_1, \ldots, n_J; m_1, \ldots, m_{J-1})$ is

$$N_D(n_1, \ldots, n_J; m_1, \ldots, m_{J-1}) = \prod_{j=1}^{J-1} C_{m_j}^{n_j} C_{n_j - m_j - 1}^{n_{j+1}-1} \tag{8}$$

where $C_m^n = \dfrac{n!}{n!(n-m)!}$.

Figure 7 demonstrates an application of equations (6) - (8). In the ray generation scheme employed by our program, the 168th kinematic group created has kinematic definition (3,2,1). Upon consulting equation (6), we see that m_1 may be 2 or 1 ($\Lambda(m_1) = 2$) and m_2 must be 1 ($\Lambda(m_2) = 1$). Therefore, the individual waves in each subgroup is found by equation (8). In figure 7 the top six rays are dynamically equivalent as are the lower six. Thus, for purposes of synthetic seismogram construction, only two amplitude computations are necessary rather than twelve. Both computations are based on one set of numerical values for interface coefficients (ray parameter is identical for the whole kinematic group) and one evaluation of geometrical spreading.

Let us now examine the amplitude-distance properties of these dynamic analogs for the model described in Table 1. A P-type head wave can propagate along the fourth interface of Figure 7 since the P wave velocity in layer 4 exceeds that in layer 3. The above classification scheme for kinematic and dynamic analogs applies equally well to head waves as to reflected waves. If we examine the dynamic properties of this kinematic group near the critical point, it will be necessary to employ the Weber function approach for interference waves.

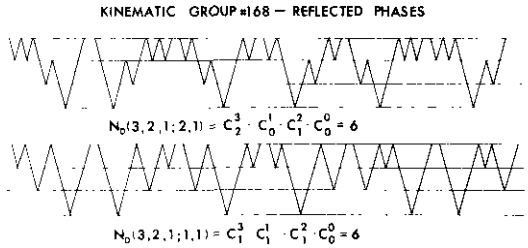

Fig. 7. Decomposition of the kinematic group (3,2,1) into two dynamic groups of six analogs each.

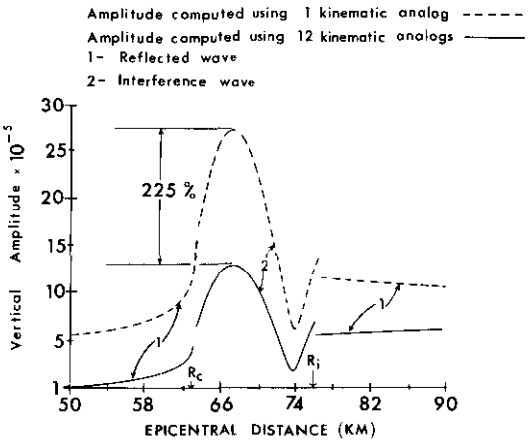

Fig. 8. Dynamic properties of the kinematic group in Model 2 as sketched in Figure 7 for a harmonic source frequency of 15 Hz. The dashed set of curves was computed by employing only one ray, while the solid set was computed by employing all twelve rays. Asymptotic ray theory was employed outside the interference zone, while the Weber function approach was used within (between R_c and R_i).

Figure 8 displays the amplitude-distance characteristics for the kinematic group sketched in the Figure 7. Within the interference zone the Weber function approach was used to evaluate the interference wave amplitude, while elsewhere asymptotic ray theory was employed. The predominant source frequency was set at 15 Hz. The two sets of curves in Figure 8 indicate the

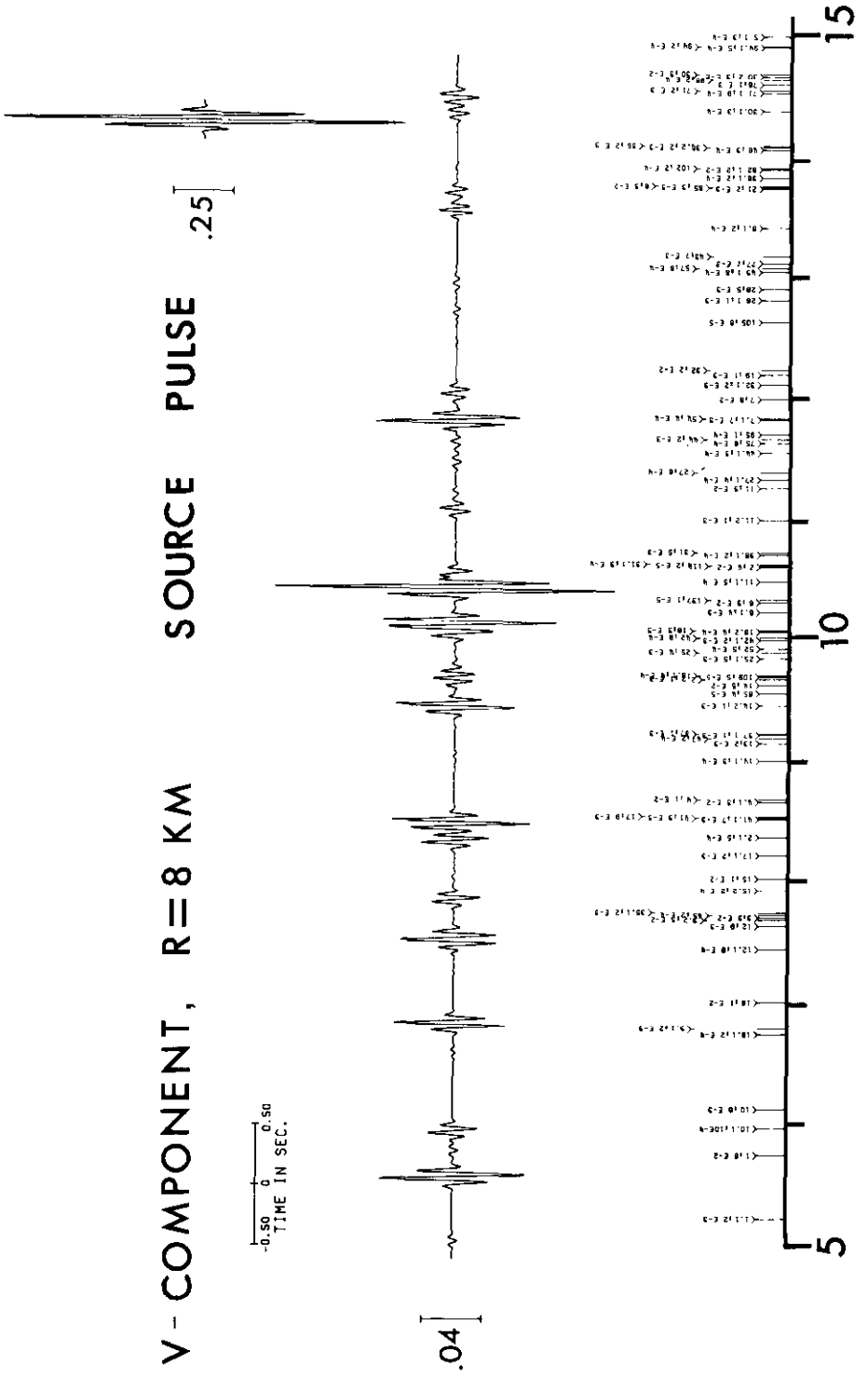

Fig. 9. Source pulse and vertical component of motion at R = 8 km computed for Model 2. Each kinematic group is identified by a code number. The relative amplitude of each group as it arrives at the receiver is shown in FORTRAN E code.

type of error that can occur when not all members of a kinematic group are considered. The dashed set of curves were produced using only one out of the twelve rays comprising the kinematic group. Due to destructive interference (remember that amplitude is in general complex-valued) between the two dynamic subgroups, the correct amplitude is somewhat less (by a factor of 225%) than that of a single ray.

The properties of kinematic and dynamic analogs, besides their impact on the effectiveness in synthetic seismogram computation , also have an important consequence on the numerical modelling of dynamic properties of individual rays and on the commonly used interpretation techniques applied to layered media with no lateral inhomogeneities of thickness variations. Since the kinematically equivalent waves cannot be separated from each other at any epicentral distance in these media, we cannot speak about arrivals or individual rays in related seismograms. This is so because nearly all (with trivial exceptions) registered wavelets are the result of interference among a number of kinematically equivalent waves.

If one were to consider converted phases, the formulation for splitting kinematic groups into dynamic subgroups becomes more involved. Formulae for these rays will not be reported here, but the interested reader is referred to Hron, Daley and Marks (1977).

SYNTHETIC SEISMOGRAMS

Asymptotic ray theory, combined with the Weber function approach and the concepts of kinematic and dynamic analogs, has been applied to a near suface impulsive point source in a plane, four-layered, elastic, homogeneous, isotropic model described in Table 2 and proposed by Kosminskaya (personal communication). The source pulse of unit amplitude was chosen to be that defined by equation (5) for a predominant frequency of 15 Hz and g=5. A display of this pulse is shown in Figure 9. The algorithms were programed in FORTRAN and applied on an Amdahl 470 V/6 computer. A CalComp plotter was used for the display.

Ray methods of studying seismic wave propagation allow the user to associate with each event on a seismogram, a particular set of kinematically equivalent rays. As well, the relative amplitude of this group which arrives at the receiver may be determined. Figure 9 also shows a vertical seismogram for Model 2 at a distance of 8 Km. The lines drawn perpendicular to the time axis indicate the arrival time of the group of kinematic analogs denoted by the number lying directly above this line. The total relative amplitude in FORTRAN E format of the group follows the identifying number. Kinematic group numbers with no digit beyond the decimal point represent reflected phases, while those with a 1 (2) beyond the decimal point denote

TABLE 2

Model 2

Layer Number	P wave Velocity km/sec	S wave Velocity km/sec	Volume density g/cm^3	Thickness km
1	1.500	0.866	2.10	3.0
2	3.000	1.732	2.75	3.0
3	6.600	3.811	2.90	8.0
4	8.000	4.619	3.40	11.0
Half-space	8.600	4.965	3.55	∞

According to Kosminskaya, 1970, personal communication.

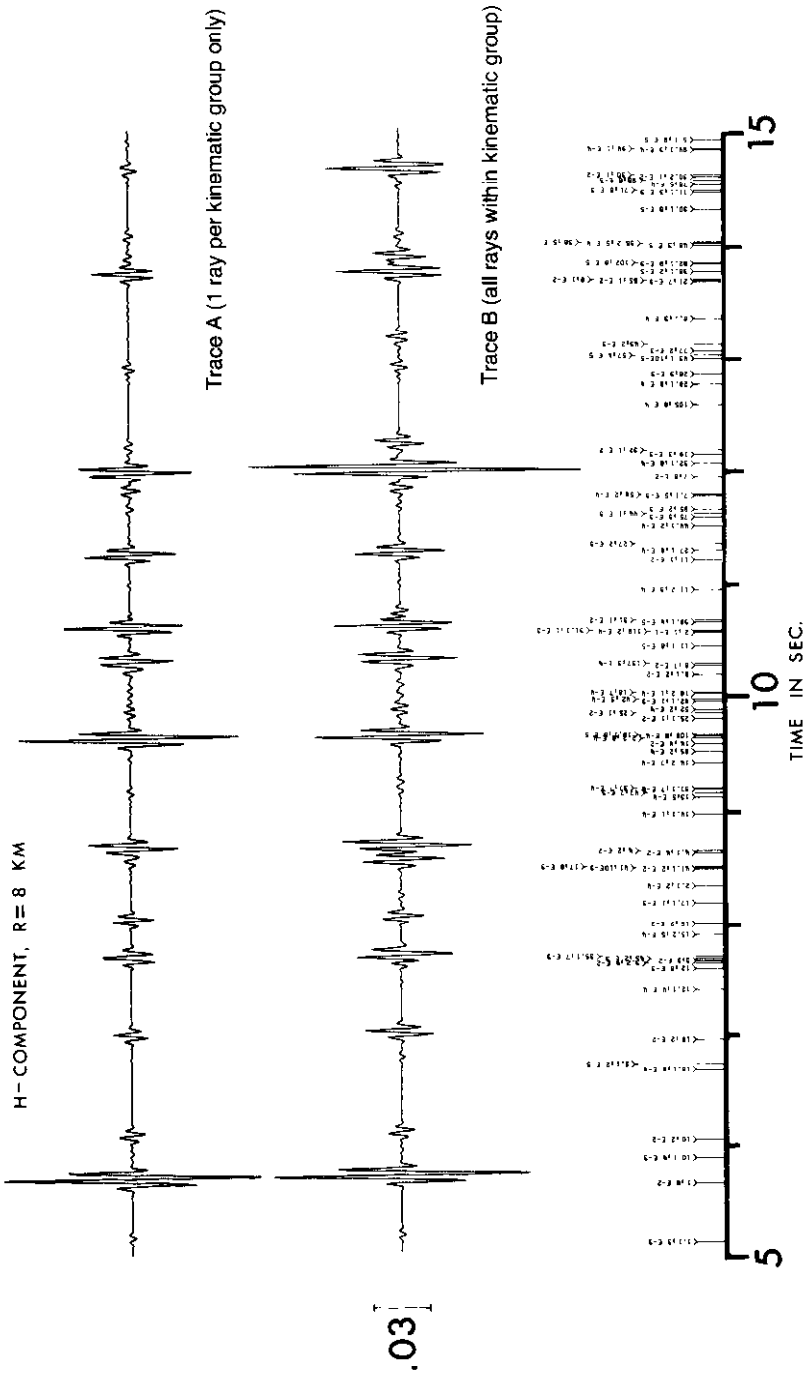

Fig. 10. Synthetic traces for Model 2 using different set of rays during computation. Trace A was computed by including only one phase per kinematic group, while Trace B included all phases. The relative amplitudes shown at the bottom are for Trace B only.

P(S)-head waves. It should be pointed out that the direct wave has been omitted from all of these seismograms as its large amplitude would require time dependent scaling. In the construction of this trace a total of 3211 phases grouped into 154 kinematic groups was created. Of these 1183 actually contributed to the seismogram. A total of 156 phases required computation of interference amplitude by the Weber function approach. Almost all of these were for phases refracted at the interface separating layers 2 and 3. The central processing unit (CPU) time required was 6.6 seconds.

A synthetic trace for the horizontal component corresponding to epicentral distance 8 km in Model 2 was computed by allowing only one representative ray contribution from each kinematic group. For some groups, this meant that up to 50 phases were neglected. The results of this computation appear as Trace A in Figure 10. Trace B was constructed by (correctly) considering all dynamic analogs. Clearly, the kinematics of Traces A and B are similar, but the wavelet shapes and amplitudes are considerably different for many events associated with more complicated ray paths. This is not suprising, since only 220 phases contributed to Trace A compared with 1183 which were utilized for Trace B.

Vertical and horizontal components of a synthetic section for Model 2 are shown in Figures 11 and 12, respectively. The arrivals are plotted with a reduced time, T-R/6.6, R being the epicentral distance. The statistics

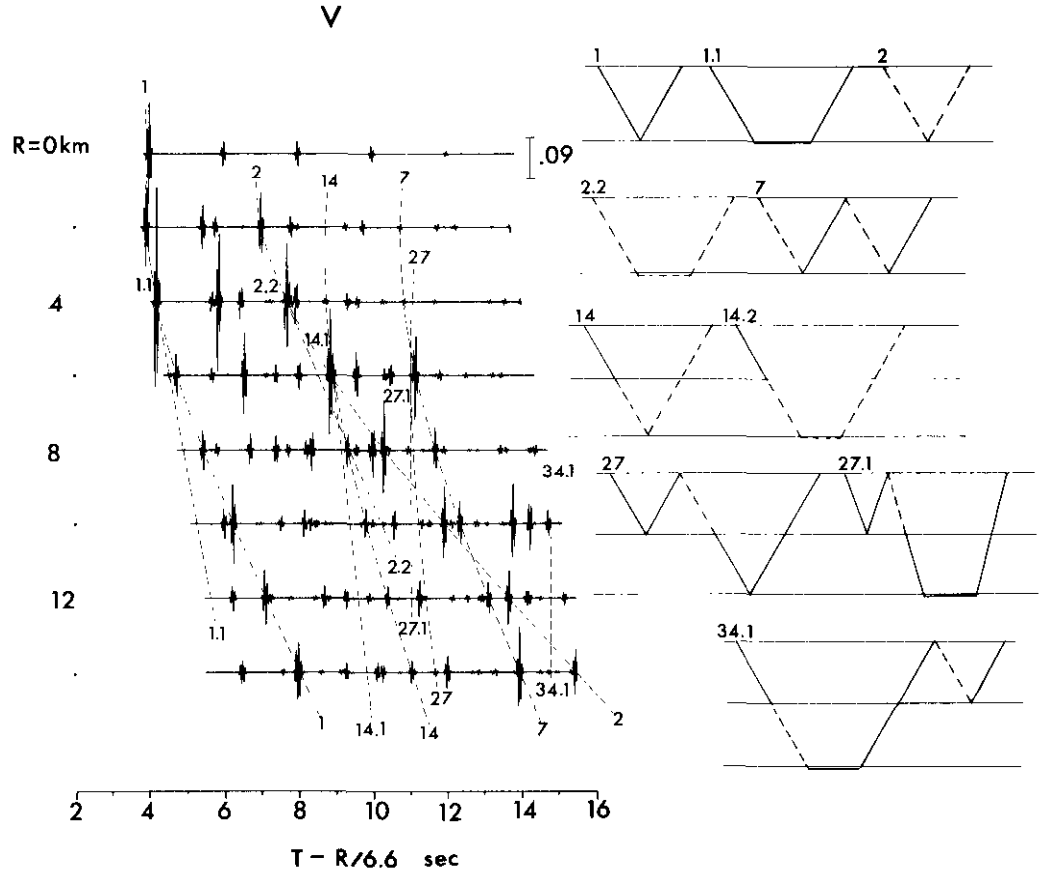

Fig. 11. Vertical component of synthetic seismograms for Model 2. Identification of some phases is shown on the right. The seismograms are displayed using a reducing velocity of 6.6 km/sec.

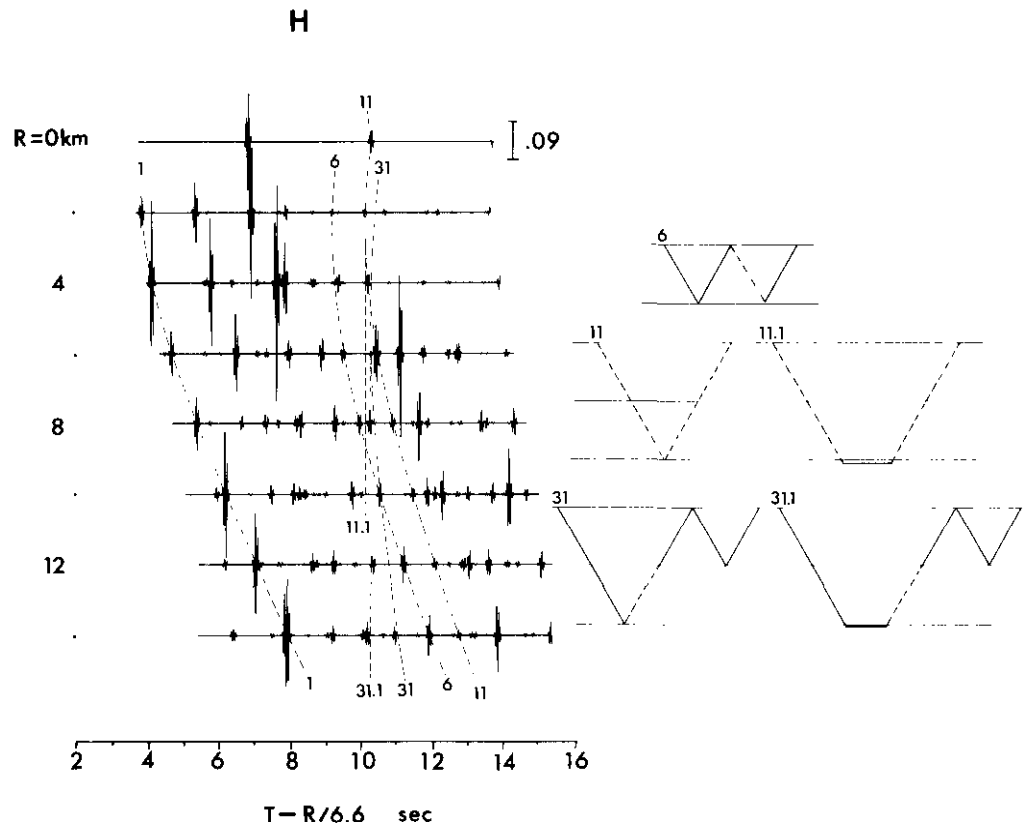

Fig. 12. Horizontal component of synthetic seismograms for Model 2 with ray diagrams of some interpreted phases.

on the phases considered and employed are roughly the same for each epicentral distance as for the traces at 8 km discussed earlier. At the right of each section are ray sketches corresponding to a few interpreted phases. Care was taken that each phase was interpreted only once. Thus, the optimum review of the results is achieved if both sets of seismograms are studied simultaneously.

CONCLUSIONS

Three methods of ray amplitude computation in homogeneous media have been presented for high frequency sources. Two of these, asymptotic ray theory and the Weber function approach, complement each other and may be used for the construction of inexpensive synthetic seismograms. Although, computationally it is the most expensive method of amplitude determination, numerical integration of the potential solutions to the wave equation provides us with the most accurate results. The Weber function approximation for interference waves near a critical point matched quite closely those predicted by the integration. Therefore, we feel that the Weber function approach is extremely useful in providing reasonably priced and correct amplitudes near critical points.

For the computation of synthetic seismograms, ray theories appear very useful. They give information about the time of arrival, the wave shape and intensity and provide the identification of the phase (and thus the ray path) pertaining to a particular event on the seismic trace. In order to properly compute synthetic seismograms one must consider a

very large set of rays as candidates for inclusion in the trace. This is best performed by a digital computer which can be programmed to group them into sets of rays with equal amplitude. Failure to consider the entire set of rays within a group makes a profound difference in the amplitude characteristics of the trace. In conclusion, the use of the concepts and techniques presented in this paper can provide an efficient and versatile means of modelling seismic wave propagation.

ACKNOWLEDGEMENTS

This study was supported by grants from the University of Alberta, the National Research Council of Canada and Imperial Oil Limited. The first author was also supported by scholarships from the SEG and the CSEG.

APPPENDIX A

ASYMPTOTIC RAY THEORY

The basic elastodynamic equation for a displacement vector $\bar{A}$ due to a disturbance in an isotropic, homogeneous medium is

$$\rho \frac{\partial^2 \bar{A}}{\partial t^2} = (\lambda+\mu)\nabla(\nabla\bar{A}) + \mu\nabla^2\bar{A} \qquad \text{(A-1)}$$

where t is time and ρ, λ and μ are the volume density and the Lamé constants. For a harmonic source of angular frequency ω, asymptotic ray theory assumes a ray solution to equation (A−1) in the form of a ray series

$$\bar{A}(\bar{x},t) = \sum_{n=0}^{\infty} \bar{A}_n(\bar{x})\, e^{-i\omega(t-\tau)}(i\omega)^{-n} \qquad \text{(A-2)}$$

where $i = \sqrt{-1}$. The $\bar{A}_n$ are the ammplitude coefficients of the ray series. The equation describing the position of the wave front at time, t, is

$$t = \tau(\bar{x}) \ .$$

For a high frequency source, the higher terms in the expansion of (A-2) approach zero rapidly. Thus, it is often sufficient to consider first terms (n=0, for reflected waves and n=1, for head waves) to obtain a viable asymptotic solution.

After substituting (A-2) into the elastodynamic equation and considering boundary conditions one obtains (for details consults Cerveny and Ravindra (1971), chapters 2-3) the amplitude of reflected waves, A_R and head waves, A_H at a distance r from the source

$$A_R = \frac{v_1}{\cos\theta_1} \frac{\prod_{m=1}^{K} R_m}{\left(\sum_{m=1}^{K} \frac{h_m v_m}{\cos\theta_m} \cdot \sum_{m=1}^{K} \frac{h_m v_m}{\cos^3\theta_m} \right)^{\frac{1}{2}}} \qquad \text{(A-3)}$$

$$A_H = \frac{v_1}{i\omega\cos\theta_1} \frac{\prod_{m=1}^{K} R_m}{\left(r(r-r^*)^3 \right)^{\frac{1}{2}}} \qquad \text{(A-4)}$$

where the following notation has been used:

v_m	velocity of propagation along m-th ray segment
θ_m	angle of incidence of the m-th ray segment upon the interface upon which it impinges
h_m	thickness of the layer housing the m-th ray segment
r^*	critical distance
K	total number of ray segments

The product term in the numerators represents the product of all reflection, transmission or head wave coefficients encountered by the ray during its propagation from source to receiver. The ray formula for head waves is not justified in the close vicinity of the critical point. This special case requires solution by wave (integral) methods and leads to amplitudes expressible in terms of a Weber function.

APPENDIX B

THE WEBER FUNCTION APPROACH FOR AMPLITUDE COMPUTATION OF THE INTERFERENCE REFLECTED-HEAD WAVE NEAR THE CRITICAL DISTANCE

The integral representing the vertical displacement due to a harmonic wave of angular frequency ω which has penetrated L layers, being reflected M times from the L+1 interface, and arrives at the free surface at an epicentral distance r is written as

$$A(r) = \frac{ik}{2} e^{-i\omega t} \int_{-\infty}^{\infty} R^M(q)\sigma(q)H_0^1(krq)e^{ikB(q)}q\,dq \qquad \text{(B-1)}$$

where we have used the following notation

$i = \sqrt{-1}$

$k = \omega/a_1$

R plane wave reflection coefficient for the L+1 interface

σ product of all other plane wave coefficients corresponding to the wave's traverse of the medium

B phase function of the wave

Hankel function of first kind and zeroth order.

After suitably deforming the contour of integration (Cerveny 1965, Cerveny and Ravindra 1971) and expanding the Hankel function for high frequencies, approximations may be applied to the integral when integrating along a portion of the steepest descent contour given by

$$(1-q^2)^{\frac{1}{2}} = (1-x^2)^{\frac{1}{2}} + pe^{-i\pi/4} \quad , -\infty<p<\infty. \quad \text{(B-2)}$$

The saddle point, x, is given by

$$\left(\frac{dB}{dq}\right)_{q=x} = r. \quad \text{(B-3)}$$

Physically, x is closely related to the constant C in Snell's law by the relation $x=a_1C=\sin\theta_1$ where θ_1 is the angle of incidence of a P wave on the first interface. For computational purposes $x=\sin\theta_1$ has been chosen as a parameter for the ray in this paper. It is clear that ray parameters corresponding to critical refraction along the L+1 interface can be written as $x_1^* = a_i/v_{L+1}$, i = 1, ...,L, where v_{L+1} is the velocity of the refracted segment of the head wave.

Due to the singularity of R at $q=x_L^*$, corresponding to the critical point in terms of the ray parameters, x, the reflection coefficient R can be conveniently decomposed as

$$R(x_L) = E(x_L) - D(x_L)S(x_L)$$

$$S = (x_L^{*2} - x_L^2)^{\frac{1}{2}} \quad H_0^{(1)} \quad \text{(B-4)}$$

where D and E depend only on even powers of S.

Performing these operations on equation (B-1) yields an expression for the displacement contribution of the reflected wave near the critical point:

$$A_R(r) = e^{-i\omega(t-t_R)} \quad \frac{\sigma(x_L)}{Q} \left\{ R^M(x_L) - M\, E^{M-1}(x_L) \right.$$

$$\left. D(x_L)c(x_L^{*2}-x_L^2)^{\frac{1}{2}} \left(\frac{g_1(\beta)}{\beta^{\frac{1}{2}}} - 1 \right) \right\} \quad \text{(B-5)}$$

where the following notation has been employed

t_R time of arrival of the reflected wave,

Q geometrical spreading of the reflected wave,

$$c = \begin{cases} 1 & \text{for P type head waves} \\ \dfrac{b_{L+1}}{a_{L+1}} & \text{for S type head waves} \end{cases}$$

$$x_i = a_1 x/a_i \quad , \qquad i = 1,\ldots,L$$

$$\beta = \left(\frac{k(r-\tilde{r})}{2x^3}\right)^{\frac{1}{2}} \left((1-x_1^{*2})^{\frac{1}{2}} - (1-x^2)^{\frac{1}{2}} \right)$$

$$g_1(\beta) = \pi^{-\frac{1}{2}} \int_{-\infty}^{\infty} (\beta - pe^{-i\pi/4})^{\frac{1}{2}} e^{-p^2} dp$$

$$\tilde{r} = x^3 \left(\sum_{i=1}^{L} \frac{N_{Pi} h_i \left(\frac{a_1^2}{a_i^2} - 1\right)}{\left(\frac{a_1^2}{a_i^2} - x^2\right)^{3/2}} + \sum_{i=1}^{L} \frac{N_{Si} h_i \left(\frac{a_1^2}{b_i^2} - 1\right)}{\left(\frac{a_1^2}{b_i^2} - x^2\right)^{3/2}} \right)$$

N_{Pi}, N_{Si} number of P and S ray segments in the i-th layer

h_i thickness of the i-th layer.

For regions beyond the critical distance, r^*, the integral in equation (B-1) has contributions from a circumvention of the branch cut given parametrically by

$$(1-q^2)^{\frac{1}{2}} = (1-x_1^{*2})^{\frac{1}{2}} + pe^{-i\pi/4}, \quad 0 \le p < \infty. \quad \text{(B-6)}$$

Physically, this may be interpreted as the head wave contribution to the displacement on the surface. Mathematically, the omission of the integration along this path would prohibit a transformation of integration contours since we would end up on a Riemann sheet different from that at the beginning of the contour. Evaluating equation (B-1) along contour (B-6) and remembering that the maximum value of the integrand occurs near p=0, gives a head wave contribution

$$A_H(r) = Me^{-i\omega(t-t_H)}\,\sigma(x_L^*)\,\Gamma\,E^{M-1}(x_L^*)c\cdot \left(\frac{x_1^*\,(1-x_1^{*2})}{8kr^2(r-\tilde{r}^*)^3}\right)^{1/4} g_2(y^*) \qquad \text{(B-7)}$$

where

t_H head wave arrival time

Γ head wave coefficient $= D(x_L^*)\,x_L^*$

$\tilde{r}^*$ $\tilde{r}$ with x_1^* substituted for x

$$y^* = \left(\frac{k\,x_1^*\,(1-x_1^{*2})}{2(r-\tilde{r}^*)}\right)^{1/2}(r-r^*)$$

$$g_2(y^*) = \pi^{-1/2}\,2^{5/2}\,e^{7i\pi/8}\int_0^\infty p^{1/2}\exp(-p^2-2e^{i\pi/4}py^*)\,dp.$$

Near the critical point we must consider the summed total response due to the head wave interfering with the reflected wave. Adding equations (B-5) and (B-7) and making approximations which are legitimate within the interference zone, gives the displacement of the interference reflected-head wave

$$A(r) = e^{-i\omega(t-t_R)}\,\frac{\sigma(x_L)}{Q}\left\{R^M(x_L) - M\Gamma c\left(\frac{(1-x_1^{*2})}{x_1^*\,k(r-\tilde{r}^*)}\right)^{1/4}\cdot E^{M-1}(x_L^*)\left(i2^{3/4}(g_1(\beta)-\beta^{1/2}) - 2^{-3/4}e^{-iy^2}g_2(y^*)\right)\right\} \qquad \text{(B-8)}$$

where $y = (\omega(t_R-t_H))^{1/2}$. Obviously, a new function G can be defined as

$$G = i2^{3/4}\left(g_1(\beta)-\beta^{1/2}\right) - 2^{-3/4}e^{-iy^2}g_2(y^*). \qquad \text{(B-9)}$$

Numerical investigation has shown that for realistic seismological models, the three parameters β, y and y^* are nearly equal within the interference zone. They can be assigned a common definition as

$$y = \begin{cases} \beta & \text{for } r<r^* \\ \left(\omega(t_R-t_H)\right)^{1/2} & \text{for } r\geq r^*. \end{cases}$$

With the introduction of $\gamma=p-ye^{i\pi/4}$ in $g_1(y)$, G (y) can be recast as

$$G(y) = -2^{3/4}\pi^{-1/2}\exp(7i\pi/8-iy^2)\int_{-\infty}^{\infty}\gamma^{1/2}\cdot \exp(-\gamma^2-2y\gamma e^{i\pi/4})\,d\gamma - i2^{3/4}y^{1/2}. \qquad \text{(B-10)}$$

This expression for G can be rewritten with the help of the integral form of the Weber function D (Magnus and Oberhettinger, 1949).

$$D_{1/2}(y(i-1)) = \pi^{-1/2}2^{1/4}\exp\left(-\frac{i}{2}y^2 - i\pi/4\right)\cdot \int_{-\infty}^{\infty}\gamma^{1/2}\exp\left(-\gamma^2-2y\gamma e^{i\pi/4}\right)d\gamma.$$

Near the critical point $S\approx 0$ in equation (B-4) and thus formula (B-8) may be simplified further by setting $E^{M-1}(x_L^*)\approx R^{M-1}(x_L^*)$. With these changes and the use of a pretabulated Weber function file, equation (B-8) lends itself to rapid evaluation on a digital computer.

REFERENCES

Berzon, I., Yepinat'eva, A., Pariskaya, G. and Starodubskaya, S., 1962, Dynamic characteristics of seismic waves in real media: Moscow, Acad. of Sciences of USSR (in Russian).

Brekhovskikh, L., 1960, Waves in layered media: New York, Academic Press.

Cerveny, V., 1962a, On reflected and head waves around the first and second critical point: Geofysikalni Sbornik, v. 165, p. 43-94.

---, 1962b, On the length of the interference zone of a reflected and head wave beyond the critical point: Studia Geophys et Geod., v. 6, p. 49-64.

---, 1965, The dynamic properties of reflected and head waves around the critical point: Geofysikalni Sbornik, v. 221, p. 135-145.

----, 1967, The theory of reflected and head waves in the case of a layered overburden: Geofysikalni Sbornik, v. 269, p. 133-180.

Cerveny, V. and Ravindra, R., 1971, Theory of seismic head waves: Toronto, Univ. of Toronto Press.

de Boor, C., 1971, CADRE: An algorithm for numerical quadrature, in, Mathematical Software, J.R. Rice, editor: New York, Academic Press.

Hron, F. 1972, Numerical methods of ray generation: Methods in computational physics, v. 12, p. 1-34.

Hron, F. and Kanasewich, E., 1971, Synthetic seismograms for deep seismic sounding studies using asymptotic ray theory: Bull. Seism. Soc. Am., v. 61, p. 1169-1200.

Hron, F., Daley, P. and Marks, L. 1977, Numerical modelling of seismic body waves in oil exploration and crustal seismology: Proceedings of 1977 ASME Symposium on Computing Methods in Geophysical Mechanics, Atlanta, ed. R.P. Shaw, AMD - v. 25, p. 21-42.

Kireyeva, I. and Karpov, K., 1961, Tables of Weber functions: London, Pergamon Press.

Magnus, W. and Oberhettinger, F., 1949, Formulas and theorems for the special function of mathematical physics: New York, Chelsea Publishing.

Marks, L., 1976, Dynamic properties of head waves near the critical point: M.Sc. thesis, University of Alberta, Edmonton.

Marks, L. and Hron, F., 1977., Weber function computation in the interference reflected-head wave amplitude: Geoph. Res. Letters, v. 4, p. 255-258.

Marks, L. and Hron, F., 1979, Dynamic properties of reflected and head waves near the critical points: submitted to Can. Jour. Earth Sciences.